Co-published by
Institute of Fluid-Flow Machinery
Polish Academy of Sciences
Committee on Thermodynamics and Combustion
Polish Academy of Sciences

http://www.imp.gda.pl/archives-of-thermodynamics/

Influence of wall temperature on condensation rate in duct flow of humid air: a comprehensive computational study

Jakub Bobrowski[a*], Artur Gutkowski[a]

[a]Lodz University of Technology, Institute of Turbomachinery, 217/221 Wólczanska, 93-005 Łódź, Poland
*Corresponding author email: 248731@edu.p.lodz.pl

Received: 06.02.2024; revised: 27.04.2024; accepted: 05.06.2024

Abstract

In engineering phase-change phenomena are found in a multitude of applications, ranging from refrigeration and air conditioning to steam turbines and petroleum refining. This study investigates the flow of moist air in a circular duct where water vapour condenses in contact with the cold wall of the duct. The investigation delves into the relationship between the condensation mass transfer rate, the heat transfer between the bulk flow and the wall, and the temperature of the wall. The volume of fluid model coupled with the Lee evaporation-condensation model was employed. Five simulations were carried out, involving different wall temperatures while maintaining the same inlet conditions. Condensation was more pronounced at lower wall temperatures, which aligns with the expectations. The heat transfer between the bulk flow and the wall decreased with the decreasing temperature difference. Interestingly, the findings revealed that the surface heat transfer coefficient increased as the wall temperature approached the temperature of the bulk flow. The success of the study suggests potential applications in optimising thermal management systems, with implications for industries where accurate predictions of moisture behaviour and heat transfer are crucial.

Keywords: Computational fluid dynamics; Volume of fluid; Heat transfer; Mass transfer; Condensation

Vol. 45(2024), No. 3, 127–133; doi: 10.24425/ather.2024.151229

Cite this manuscript as Bobrowski, J., & Gutkowski, A. (2024). Influence of wall temperature on condensation rate in duct flow of humid air: a comprehensive computational study. *Archives of Thermodynamics*, 45(3), 127–133.

1. Introduction

Phase changes are ubiquitous in our everyday lives and play a fundamental role in various applications across diverse fields. In engineering, the controlled evaporation and condensation of working fluids are found in a multitude of applications, offering innovative solutions to various challenges. One prominent example can be found in the field of refrigeration and air conditioning. These systems rely on the evaporation and subsequent condensation of a refrigerant to regulate temperatures. The working fluid evaporates within the evaporator coils, absorbing heat from the surrounding environment, thereby cooling the space. The vapourised refrigerant is then compressed, releasing the absorbed heat, and subsequently condensed back into a liquid in the condenser [1,2]. The applicability of phase changes extends beyond refrigeration and air conditioning. Many power plants, both nuclear and fossil fuel-based, use steam turbines to generate electricity. Water is heated to produce high-pressure steam, which drives turbines, and then the steam is condensed back into water, completing a continuous cycle [2]. This phase change mechanism is fundamental to power generation. Another good example of this is distillation, a process which takes advantage of the different characteristics of the substances in a mixture in order to separate them. In the petroleum industry,

Nomenclature

h – surface heat transfer coefficient, W/(m^{2}K)
I – turbulence intensity
M – mass transfer rate, kg/s
n – power-law exponent
P – pressure, Pa
q – heat flux, W/m^2
Q – heat transfer rate, W
r – radial coordinate, m
R – radius of the pipe, m
Re – Reynolds number
RH – relative humidity
T – temperature, K
u – axial velocity, m/s

Subscripts and Superscripts

avg – average
c – condensation
max – maximum value
ref – reference condition
sat – saturation condition
v – vapour
wall – through the wall/on the wall

Abbreviations and Acronyms

RANS– Reynolds averaged Navier-Stokes
VOF – volume of fluid

distillation is used to extract products like liquid petroleum gas and gasoline from crude oil. Similarly, within the alcohol industry, distillation is in the centre of the production of distilled spirits.

Numerous experimental and numerical investigations have been conducted on phase change phenomena. In [3], the volume of fluid method (VOF), coupled with an in-house evaporation-condensation mass transfer model, was employed by the authors to explore phase changes in the internal two-phase flow of R134a refrigerant. The findings showed reasonable agreement with available experimental data. In [4], the condensation of water vapour in the presence of dry air was examined by the authors, who employed two advection equations to monitor the free surface and utilised the Lee model to simulate interfacial mass transfer. The results demonstrated favourable alignment with experimental data, revealing a nearly linear decrease in condensation rate as the dry air mass fraction increased. In the paper [5], the authors delved into the evaporation of a water film in a duct with a humid air flow, where the volume of fluid and Lee model were employed to capture the physics. The evaporation rate was observed to rise with the increasing air temperature and decreasing air flow rate. In [6], a single-phase approach was developed by the authors to model the condensation of vapour in the presence of air, yielding good agreement with experimental data. Interesting conclusions were drawn in [7], where the authors investigated the influence of flow direction on the condensation process in a vertical pipe. The study developed a mathematical model based on conservation equations and validated it through experimental apparatus. Results suggested that co-current gas/liquid flow enhanced heat transfer. Additionally, comparisons between theoretical predictions and experimental findings confirmed the model's accuracy.

In this study, the numerical simulation explores the flow of humid air in a circular duct, where water vapour condenses in contact with the cold wall of the duct. The objective is to evaluate how the wall temperature influences the condensation mass transfer rate of water vapour in the presence of dry air.

2. Materials and methods

The model was prepared and solved within the commercial computational fluid dynamics (CFD) package Ansys Fluent. To simulate this case, the steady-state Reynolds-averaged Navier-Stokes (RANS) approach was adopted, offering a balanced compromise between accuracy and computational cost. RANS modelling stands as the industry standard for heat transfer and mass transfer applications. It has proven to be quite successful at predicting both local and integral quantities in heat and mass transfer applications [4,6,8].

Five simulations were carried out, involving different wall temperatures while maintaining the same inlet conditions, as detailed in Table 1.

Table 1. Simulations.

Simulation number	Inlet conditions	Wall temperature [K]
1	u_{avg} = 3.91 m/s Re = 10^4 T = 303.15 K RH = 95%	278.15
2		283.15
3		288.15
4		293.15
5		298.15

The fluid domain is a cylindrical space bounded by the duct with a standard diameter of 40 mm. In the hypothetical real-life laboratory, the duct extends sufficiently far upstream from the inlet (Fig. 1) for the velocity profile to fully develop and for the

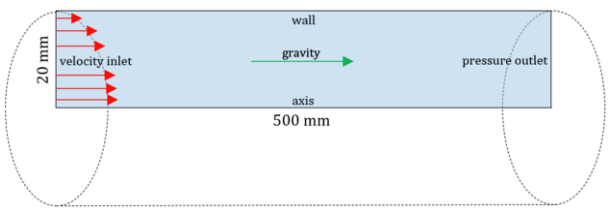

Fig. 1. Boundary conditions.

temperature distribution to plateau, achieving the inlet conditions specified in Table 1. Although the duct is quite lengthy, in this context, focus is put on a segment that is 500 mm in length, whose walls are maintained at a temperature different from that of the upstream part. The copper duct releases heat through forced convection to the surroundings. An external liquid-cooling system is used to maintain a uniform temperature of the segment. Downstream from the outlet, the flow exits into atmospheric conditions. It is important to observe that the shape of the domain, the boundary conditions, and the expected results exhibit axisymmetry (the water condenses as an axisymmetric film because asymmetric dropwise condensation requires vapour additives or surface coatings to maintain, and often transitions to film condensation over time [1]). Hence, the problem can be visualised on the axial-radial plane, where the third circumferential dimension has no impact on the results. With this in mind, the three-dimensional cylinder was simplified into a single rectangular shape measuring 20 mm by 500 mm, as shown in Fig. 1.

Because of limited computational resources, a decision was made to use a coarse discretisation in the bulk flow and utilise mesh adaptation to refine the grid in the near-wall region, thereby increasing both flow-wise and wall-normal resolution. The final mesh is based on a rectangular grid that has 30 cells in the radial direction with a bias factor of 10 000 (creating a decreasing cell height towards the wall) and 50 equally-distributed divisions along the length of the duct. Hanging node mesh adaption [9] was used afterwards. In contrast to mesh refinement achieved by increasing the bias factor or the number of divisions, this approach mitigates the occurrence of excessive aspect ratios in near-wall cells. The refinement region extends approximately 5 mm from the wall (as shown in Fig. 2), reaching well beyond the momentum, thermal and concentration boundary layer. Such discretisation results in approximately 20 cells across the thickness of the water film, which, combined with the carefully chosen numerical schemes, results in an accurate resolution of the near-wall region. The grid has a total of 5400 finite volumes.

The dry air and water vapour mixture was modelled with the use of species transport, treating both species as ideal gases. Although water vapour is close to the saturation line, it can be effectively treated as an ideal gas under such low pressures [2]. Moreover, dry air and water vapour properties exhibit negligible variations within the temperature ranges applied. Since the mass fraction of water vapour is minimal and the properties of water vapour and dry air are rather similar (except for the specific isobaric heat capacity, which is twice as large for water vapour), the properties of humid air were assumed to be identical to those of dry air. Careful consideration was given to the temperature point at which these properties were obtained. While the bulk flow has a temperature of 303.15 K, heat and mass transfer phenomena occur in the colder near-wall region. Hence, the properties of dry air were extracted from tables [10,11] for a temperature of 293.15 K, a value in-between the hot core of the flow and the cold wall. The properties of the mixture are tabulated in Table 2. The molar heat of condensation was set to 4.4×10^7 J/kmol [12].

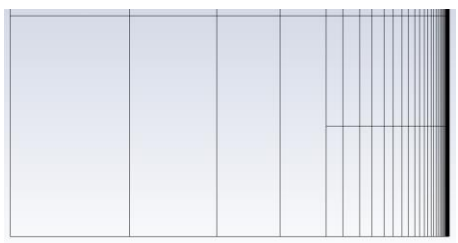

Fig. 2. Grid refinement (radial direction to the right).

Liquid water was modelled as an incompressible fluid. While most of its properties (shown in Table 2) exhibit meagre temperature dependence, the dynamic viscosity of water changes drastically with temperature [13]. In each simulation, the viscosity of water was taken from tables [14] for the temperature of the wall, as tabulated in Table 3.

The closure of the RANS equations was achieved by employing the shear stress transport (SST) turbulence model. Based on the Boussinesq concept of eddy viscosity, this model proves effective for shear flows dominated by one of the turbulent shear stresses, as seen in pipe flows. Moreover, the SST model allows for full boundary layer resolution, a crucial aspect for found widespread use in similar contexts [6, 15,16]. Turbulence damping was implemented to limit unrealistic turbulence production within the interfacial region and help capture the velocity field near the free surface [17–19].

Table 2. Humid air and water properties.

Property	Humid air	Water liquid
Density [kg/m³]	Ideal gas law	1000
Thermal conductivity [W/(K m)]	0.025	0.60
Dynamic viscosity [kg/(m s)]	1.8×10^{-5}	See Table 3
Specific isobaric heat capacity [J/(kg K)]	1000	4200
Mass diffusivity of water vapour in large excess of dry air [m²/s]	2.4×10^{-5}	NA

Table 3. Water liquid dynamic viscosity as a function of temperature.

Wall temperature [K]	Water liquid dynamic viscosity [10^{-3}×kg/(m s)]
278.15	1.5
283.15	1.3
288.15	1.1
293.15	1.0
298.15	0.89

The inlet velocity was defined as a velocity profile, established through the power-law approximation:

$$u(r) = u_{max}\left(1-\frac{r}{R}\right)^{1/n}. \quad (1)$$

For the calculated Reynolds number, the exponent n was estimated to be 5.3 [20].The turbulence properties at the inlet were

provided implicitly in terms of the hydraulic diameter and turbulence intensity, in accordance with the Fluent guidelines [19]. From the equation [19,21]

$$I = 0.16\,\mathrm{Re}^{-1/8}, \tag{2}$$

the inlet turbulent intensity was estimated to be 5%.

A gauge pressure of 0 Pa was specified at the outlet, and the reference pressure was set to 101 325 Pa.

The temperature on the outer side of the wall specified as a parameter T_{wall}, and the thermal resistance of the wall was defined based on a thickness of 2 mm and the thermal conductivity of copper, which is 390 W/(m K).

In the examined scenario, water vapour experiences local cooling in proximity to the walls, leading to its condensation as a liquid film [1]. This represents a case of stratified flow, where phases are separated into distinct layers with a well-defined interface. The VOF model, designed for such applications [9], was employed in this study. The model has found widespread use in modelling multiphase flows [3–5,8].

The implicit scheme was used, wherein the phase continuity equation is solved iteratively together with momentum and pressure [18]. The interface modelling type was set to 'Sharp', the preferred option for distinct and well-defined interfaces between phases [19]. Although interfacial anti-diffusion is typically suggested for sharp interfaces resolved on meshes with high aspect ratios [18,19], it was deliberately left inactive. This decision was made due to the recommendation for allowing some numerical diffusion when the evaporation-condensation mass transfer mechanism is enabled [19]. Since gravitational forces acting on the water film are significant, the 'Implicit Body Force' formulation was enabled, in accordance with [17,19].

The evaporation-condensation approach utilised the Lee model, with the evaporation and condensation coefficients set to 10 and 20 000, respectively, in accordance with [22]. This model is widely used in modelling interfacial mass transfer [3–6,8].

The saturation temperature was defined as a function of water vapour pressure through a 'User Defined Function'. It utilises the Antoine equation to compute and return the saturation temperature [23,24]:

$$T_{sat} = \frac{B}{A - \log_{10}\frac{P_v}{10^5\ \mathrm{Pa}}} - C + 273.15\ \mathrm{K}. \tag{3}$$

For water, the equation parameters are approximately as follows: A = 5.1156, B = 1687.5 and C = 230.17. These parameters have been fine-tuned for use within the temperature range of 273 K to 473 K and under pressures ranging from 1 kPa bar to 1600 kPa [24]. Although the current set of coefficients is applicable for vapour pressures greater than 1 kPa, its range of applicability in this study can be expanded. At 1 kPa, the calculated saturation temperature is 280 K, a value that approaches the lower limit of the thermal range observed within the pipe. Under lower pressures, the calculated saturation temperature decreases below the minimum temperature within the domain (regardless of whether the formula overestimates or underestimates the result), thereby maintaining a gaseous state in the respective cells.

The solver was run in the double-precision mode, the recommended approach for high-aspect-ratio meshes [19]. The simulation employed a pressure-based, steady-state solver with enabled pressure-velocity coupling, following the guidelines outlined in [9]. Moreover, the 'Coupled with Volume Fractions' option was enabled. The pressure interpolation scheme was set to 'Modified Body Force Averaged', which provides better stability for multiphase flows with body forces compared to its alternatives [9]. Additionally, the gradient reconstruction scheme was selected as 'Least Squares Cell Based', following the recommendation outlined in [9]. The spatial discretisation of momentum, turbulence, density, energy and species transport equations was set to 'Second Order Upwind'.

The volume fraction interface scheme was set to 'Modified HRIC'. While offering inferior interface resolution compared to the compressive scheme [18], a more diffusive discretisation is recommended when the evaporation-condensation mass transfer mechanism is enabled [19].

'Pseudo-Transient' under-relaxation was activated. This approach not only accelerates the convergence of steady-state problems but can also assist in the convergence of mildly unsteady flows [17].

To assess iterative and spatial convergence, the approach involved monitoring equation residuals and five integral output quantities: the water mass flow rate through the outlet, the total water film mass, the condensation mass transfer rate, the average total specific enthalpy at the outlet, and the total heat transfer rate through the wall. Both the residuals and the monitors flatlined, indicating iterative convergence. Moreover, the global balance of air/water mass and energy was verified. The grid was refined near the wall to guarantee maximum accuracy within the constraints of available computational resources.

3. Results and discussion

The results presented below are from the first simulation with a wall temperature of 278.15 K. The results from the subsequent simulations exhibit the same tendencies, differing only in values due to the progressively higher wall temperature.

The radial distribution of the mass fraction of water vapour is shown in Fig. 3 (plotted on the inlet, outlet as well as 100 mm, 200 mm, 300 mm and 400 mm from the inlet). It is evident that the vapour content consistently decreases along the stream. The most significant decline occurs just downstream from the inlet, coinciding with the steepest slope of the water film thickness (Fig. 8).

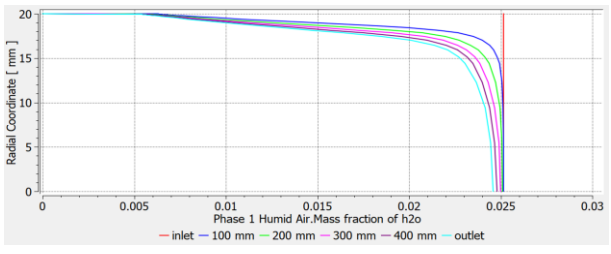

Fig. 3. Water vapour mass fraction profiles (for T_{wall} = 278.15 K).

The reduction in water vapour content results in the buildup of dry air near the wall. The presence of a non-condensable gas, such as dry air, has an adverse effect on condensation heat transfer [1]. This can be explained as follows: upon condensation of vapour mixed with a non-condensable gas, only the non-condensable gas is present near the wall. This gas layer serves as a barrier between the vapour and the surface. The vapour now has to diffuse through the non-condensable gas before reaching the surface, leading to a decreased mass and heat transfer rate.

The effectiveness of heat transfer between a fluid and a solid surface can be quantified by the surface heat transfer coefficient [19]:

$$h = \frac{q_{wall}}{T_{ref} - T_{wall}}. \quad (4)$$

It represents the rate of heat transfer per unit area per unit temperature difference between the surface and the fluid. The higher the heat transfer coefficient, the more effectively heat is transferred between the surface and the fluid.

Here, the reference temperature T_{ref} is set equal to the inlet temperature of 303.15 K. Using the average temperature on the axis, which would appear more representative of the bulk temperature, yields nearly identical results.

The presence of air, coupled with the increasing water film thickness (which can be treated as a conductive resistance due to its laminar nature [25]) and an increasing thermal boundary layer thickness, impedes heat transfer between the hot stream and the surroundings of the duct. This tendency is visible in Fig. 4. The surface heat transfer coefficient decreases in the downstream direction as both the thermal boundary layer and the water film grow.

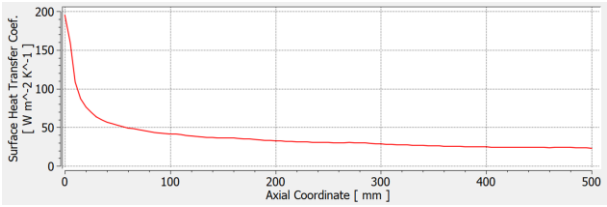

Fig. 4. Surface heat transfer coefficient along the pipe (for T_{wall} = 278.15 K).

The tendencies described above are evident in all five simulations. Some interesting patterns emerge when comparing the results for different wall temperatures. An approximately linear increase in the surface heat transfer coefficient is observed as the wall temperature approaches the freestream temperature, as shown in Fig. 5.

In free convection (single-phase flow with constant fluid properties), the heat transfer coefficient tends to increase with a growing temperature difference between the wall and the bulk flow. However, this correlation is not prominent in forced convection [25]. It can be concluded that the variability in the surface heat transfer coefficient is, to a great extent, caused by condensate formation. This trend can be explained as follows: at a higher wall temperature, the water film becomes thinner due to both reduced water viscosity and a lower condensation rate.

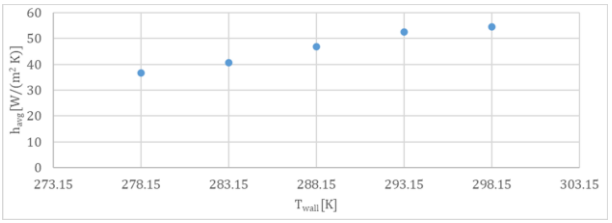

Fig. 5. Average surface heat transfer coefficient as a function of wall temperature.

A thinner water film poses less resistance to heat flow, resulting in the observed increase in the surface heat transfer coefficient.

To validate this hypothesis, simulations or experiments need to be conducted, as no correlations between the heat transfer coefficient and the temperature difference were identified in the literature.

Despite the variation in the surface heat transfer coefficient, the negative relationship between the total heat transfer rate and the temperature difference remains observable, as depicted in Fig. 6. Heat transfer becomes null when the wall temperature equals the temperature of the flow, as indicated on the graph with point T_{wall} = 303.15 K, manually added for clarity.

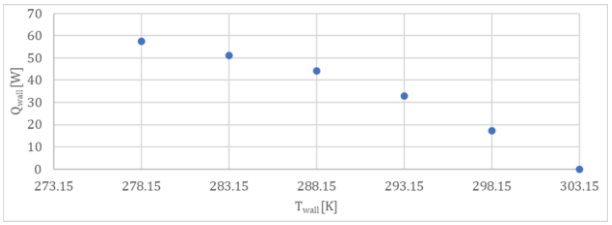

Fig. 6. Total heat transfer rate through the wall as a function of wall temperature.

While the surface heat transfer coefficient follows an intriguing trend, the variation in the condensation mass transfer rate aligns with expectations. The condensation mass transfer rate steadily decreases as the temperature of the wall increases, as can be observed in Fig. 7. No condensation would occur if the temperature of the wall and the flow were equal, as marked by the manually added point T_{wall} = 303.15 K.

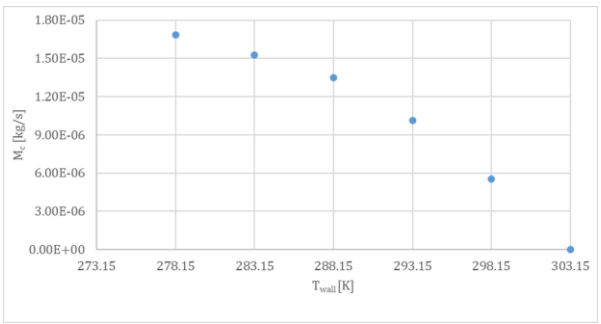

Fig. 7. Condensation mass transfer rate as a function of wall temperature.

With increasing temperature, the air's moisture-holding capacity increases. Eventually, mass transfer between the phases ceases when the temperature near the free surface reaches the dew-point temperature of the bulk flow.

As the rate of mass transfer through condensation diminishes, the water film contracts, as illustrated in Fig. 8. The reduction in thickness with each simulation is further intensified by a decrease in the viscosity of the liquid water.

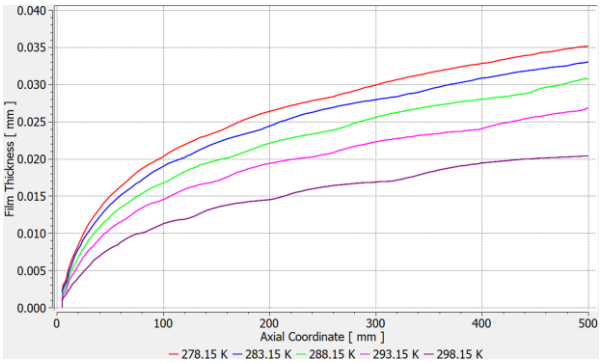

Fig. 8. Water film thickness as a function of wall temperature.

The undulating shape of the profiles is a result of how the software interpolates the value of liquid volume fraction within each computational cell. As an illustration, an interfacial cell may have a value of 0.6, while the radially adjacent cells have values of 0 and 1. An interpolation is required to determine the theoretical position of a point with a value of 0.5 (used as an iso-value to plot the film thickness). The accuracy of this interpolation largely depends on the spatial resolution of the interfacial region.

4. Summary

Throughout this study, a computational fluid dynamics model was developed to simulate the flow of moist air in a circular duct, where moisture condenses upon contact with the cold wall of the duct.

The volume of fluid surface-tracking model, ideal for stratified flows, was applied to model the free surface. The Lee model was used to compute the interfacial mass transfer through condensation, with model coefficients drawn from the literature. Additionally, a 'User-Defined Function' was developed in the C programming language to set the saturation temperature as a function of vapour pressure using the Antoine equation.

The dry air and water vapour mixture was modelled using species transport, treating both species as ideal gases with constant fluid properties. Liquid water was modelled as an incompressible fluid, with constant properties and a viscosity that was constant but different for each simulation.

The closure of the Reynolds-averaged Navier-Stokes equations was achieved by employing the shear stress transport turbulence model recommended for most industrial applications. Based on the Boussinesq concept of eddy viscosity, the shear stress transport formulation leverages the strengths of two widely adopted turbulence models: k-ω and k-ε.

Five simulations were carried out, involving different wall temperatures while maintaining the same inlet conditions. Condensation was more pronounced at lower wall temperatures, which aligns with expectations. The heat transfer between the bulk flow and the wall decreased with the increasing wall temperature. Interestingly, the findings revealed that the surface heat transfer coefficient increased as the wall temperature approached the temperature of the bulk flow.

The findings, particularly the observation that surface heat transfer coefficient increases with the decreasing temperature difference between the wall and the bulk flow, contribute to a deeper understanding of heat exchange processes. The success of the study suggests potential applications in optimising thermal management systems, with implications for industries where accurate predictions of moisture behaviour and heat transfer are crucial.

References

[1] Cengel, Y.A. (2002). *Heat Transfer: A practical approach*. McGraw-Hill.

[2] Cengel, Y.A., Boles, M A., & Kanoğlu, M. (2011). *Thermodynamics: An engineering approach*. McGraw-Hill.

[3] Ganapathy, H., Shooshtari, A., Choo, K., Dessiatoun, S., Alshehhi, M.M.M.O., & Ohadi, M. (2013). Volume of fluid-based numerical modeling of condensation heat transfer and fluid flow characteristics in microchannels. *International Journal of Heat and Mass Transfer*, 65, 62–72. doi: 10.1016/j.ijheatmasstransfer.2013.05.044

[4] Phan, T.H., Won, S.S., & Park, W.G. (2018). Numerical simulation of air-steam mixture condensation flows in a vertical tube. *International Journal of Heat and Mass Transfer*, 127, 568–578. doi: 10.1016/j.ijheatmasstransfer.2018.08.043

[5] El Baamrani, H., Bammou, L., Aharoune, A., & Boukhris, A. (2021). Volume of fluid (VOF) modeling of liquid film evaporation in mixed convection flow through a vertical channel. *Mathematical Problems in Engineering*, 2021, 9934593. doi:10.1155/2021/9934593

[6] Kumar, G.V., Cammiade, L.M., Kelm, S., Prakash, K.A., Groß, E.M., Allelein, H.J., & Rohlfs, W. (2021). Implementation of a CFD model for wall condensation in the presence of non-condensable gas mixtures. *Applied Thermal Engineering*, 187, 116546. doi: 10.1016/j.applthermaleng.2021.116546

[7] Pele, C., Baudoin, B., & Barrand, J.P. (1994). Effect of humid air flow rate on the filmwise condensation inside a vertical cooled pipe: numerical and experimental study. *International Journal of Heat and Mass Transfer*, 37(13), 1829–1837. doi: 10.1016/0017-9310(94)90323-9

[8] Szijártó, R., Badillo, A., Ničeno, B., & Prasser, H.M. (2017). Condensation models for the water–steam interface and the volume of fluid method. *International Journal of Multiphase Flow*, 93, 63–70. doi: 10.1016/j.ijmultiphaseflow.2017.04.002

[9] Ansys Inc. (2022). *Ansys Fluent theory guide*.

[10] https://www.engineersedge.com/physics/viscosity_of_air_dynamic_and_kinematic_14483.htm [accessed 25 Dec. 2023].

[11] https://www.engineeringtoolbox.com/air-diffusion-coefficient-gas-mixture-temperature-d_2010.html [accessed 25 Dec. 2023].

[12] https://www.engineeringtoolbox.com/water-properties-d_1573.html [accessed 20 Nov. 2023].

[13] https://www.engineersedge.com/physics/water__density_viscosity_specific_weight_13146.htm [accessed 25 Dec. 2023].

[14] https://wiki.anton-paar.com/en/water/ [accessed 25 Dec. 2023].
[15] Widiawaty, C.D., Siswantara, A.I., Gunadi, G.G.R., Pujowidodo, H., & Syafei, M.H G. (2020). A CFD simulation and experimental study: predicting heat transfer performance using SST k-ω turbulence model. *IOP Conference Series: Materials Science and Engineering*, 909(1), 012004. IOP Publishing.
[16] Močnik, U., Blagojevič, B., & Muhič, S. (2020). Numerical analysis with experimental validation of single-phase fluid flow in a dimple pattern heat exchanger channel. *Journal of Mechanical Engineering/Strojniški Vestnik*, 66(9), 544–553. doi: 10.5545/sv-jme.2020.6776
[17] Pawłucki, M., & Kryś, M. (2020). *CFD for engineers*, Gliwice: Helion (in Polish).
[18] Ansys Inc. (2015). *Multiphase modeling using ANSYS Fluent*.
[19] Ansys Inc. (2022). *Ansys Fluent user's guide*.
[20] https://www.nuclear-power.com/nuclear-engineering/fluid-dynamics/turbulent-flow/power-law-velocity-profile-turbulent-flow/ [accessed 21 Nov. 2023].
[21] https://www.cfd-online.com/Wiki/Turbulence_intensity [accessed 21 Nov. 2023].
[22] Lee, W.H. (1980). A pressure iteration scheme for two-phase flow modeling. In *Multiphase Transport Fundamentals, Reactor Safety, Applications* (T.N. Veziroglu, ed.), (pp. 407–431). Hemisphere.
[23] Antoine, M.C. (1888). Nouvelle relation entre les tensions et les temperatures. *C. r. held Seanc. Acad. Sci. Paris*, 107, 681–684.
[24] Poling, B.E., Prausnitz, J.M., & O'connell, J.P. (2001). *The properties of gases and liquids*: Vol. 5. Mcgraw-Hill.
[25] Welty, J., Rorrer, G.L., & Foster, D.G. (2020). *Fundamentals of momentum, heat, and mass transfer*. John Wiley & Sons.